Meshless Simulation with the Material Point Method

A Micropump for Nerve Injury Treatment

de Jong, S. D.M.; Aprea, E.; Boutry, C. M.; van Driel, W. D.

DOI
10.1109/EuroSimE65125.2025.11006580

Publication date
2025

Document Version
Final published version

Published in
Proceedings - 2025 26th International Conference on Thermal, Mechanical and Multi-Physics Simulation and Experiments in Microelectronics and Microsystems, EuroSimE 2025

2025 26th International Conference on Thermal, Mechanical and Multi-Physics Simulation and Experiments in Microelectronics and Microsystems (EuroSimE) | 979-8-3503-9300-2/25/$31.00 ©2025 IEEE | DOI: 10.1109/EUROSIME65125.2025.11006580

Meshless Simulation with the Material Point Method: A Micropump for Nerve Injury Treatment

1st S.D.M. de Jong
Department of Microelectronics
Delft University of Technology
Delft, Netherlands
S.D.M.deJong@tudelft.nl

2nd E. Aprea
Department of Microelectronics
Delft University of Technology
Delft, Netherlands
E.Aprea@tudelft.nl

3rd C.M. Boutry
Department of Microelectronics
Delft University of Technology
Delft, Netherlands
C.M.F.Viellard-Boutry@tudelft.nl

4th W.D. van Driel
Department of Microelectronics
Delft University of Technology
Delft, Netherlands
Signify
Eindhoven, Netherlands
willem.van.driel@signify.com

***Abstract*—A meshless method is used to simulate the Fluid-Structure Interaction (FSI) in a micropump intended to treat nerve injury. Conventional meshbased methods can suffer from mesh deformation and quality issues, and find it difficult to track the fluid-structure interface. The Material Point Method (MPM) combines Lagrangian material points with an Eulerian computational grid, thereby avoiding any mesh related problems. To simulate the valve dynamics in the micropump, MPM was used to analyze the effect of the valve length on the behaviour of the pump. A longer valve length takes longer to open, as it sticks to the valve seat, meaning the pump needs to generate more pressure to open the valve. This contribution shows that MPM simulations can be used to optimize the valve design for implantable micropumps.**

***Index Terms*—Fluid-Structure Interaction, Meshless, Micropump**

I. Introduction

The use of simulations in the field of MEMS is widespread [1]–[3]. Simulations are used in the design phase [4], [5] to optimize the device's performance and create faster, cheaper, and better devices. Moreover, they represent a great way to find the balance among strict design requirements. The modeling techniques used for the simulations are primarily meshbased methods such as the Finite Element Method (FEM) [6], or in some cases, the Finite Volume Method (FVM) [7]. These meshbased methods have been used with great success over the years, but they are not without issues. Firstly, creating a mesh of sufficient quality requires the time and effort of an experienced engineer. Secondly, even when a high quality is created, for large deformation problems the mesh will deform to such an extent that the simulation results will become inaccurate [8]. Techniques such as remeshing can mitigate the effects of mesh deformations, but implementing remeshing means the simulation now has to first create the new mesh, interpolate the information from the old mesh to the new mesh, and then perform the computation. Therefore, the total cost of the simulation, i.e. including remeshing, is greatly increased for large deformation problems [9]. Additionally, the mapping from the old to the new mesh can cause significant convergence problems [10]. Furthermore, it leaves questions about the quality of the newly generated mesh, as individually checking every mesh for long simulations is infeasible. Thirdly, when dealing with Fluid-Structure Interactions (FSI), meshbased methods struggle to track the fluid-structure interface. The position and morphology of the interface must be accurately tracked to obtain accurate simulation results. To circumvent these issues stemming from the mesh, a meshless method can be used instead. As the name suggests, meshless methods do not make use of a mesh, so any mesh related problems do not occur. Various meshless methods are available, such as Smooth Particle Hydrodynamics (SPH) [11], Radial Basis Functions (RBF) [12] or Moving Particle Semi-implicit (MPS) [13], but in this work the Material Point Method (MPM) is employed. Originally introduced by Sulsky et al. [14] for simulating solid mechanics. It was based on the Particle In Cell (PIC) [15] method used for modeling fluid mechanics. The MPM is therefore eminently suited for simulating fluid-structure interactions, and it has been employed successfully [16]–[18]. The MPM scheme consists of a set of Lagrangian points imposed on a Eulerian grid. Information is mapped from the points to the grid, where the grid momentum is updated and transferred back to the points. This ensures there is no direct interaction between the points, allowing them to move freely. Because MPM does not need any remeshing when simulating large deformation problem, the total cost of the simulation can be lower when compared with FEM simulations [9], [19], making MPM a more efficient method for simulating large deformation problems. Additionally, the tracking of the interface can be performed using the points on the interface, allowing for accurate tracking of the fluid-structure interface [17].

979-8-3503-9300-2/25/$31.00 ©2025 IEEE Presented at the EuroSimE 2025 Conference

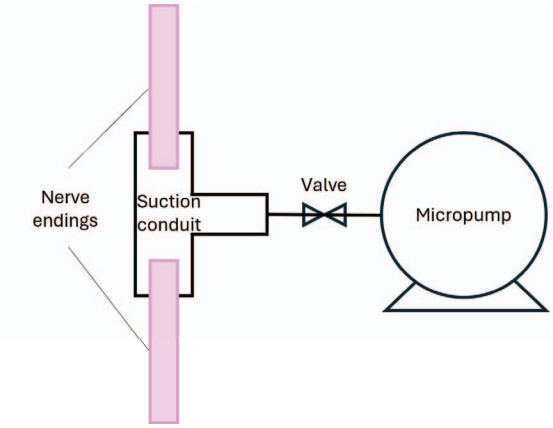

Fig. 1: A schematic showing how the nerve ends are connected to the micropump.

In this contribution, the material point method is used to model the micropump to showcase its capabilities. The micropump under consideration is a MEMS device designed to be implanted in the body to provide under-pressure, thereby stimulating peripheral nerve regrowth after Peripheral Nerve Injury (PNI). Around 300,000 individuals are impacted by PNI each year in Europe alone [20]. Traditional treatments, like autografting and nerve entubulation, demonstrate limited effectiveness [21], thus a full recovery is often impossible [22]. However, research indicates that applying under-pressure to the proximal and distal nerve ends in mice can significantly improve nerve recovery [23]. A schematic representation of the device is provided in Fig. 1. A conduit is attached to the damaged nerve ending, to which an under-pressure is provided by the micropump. A valve prevents any backflow into the conduit, so it can maintain the desired pressure. As the micropump aims to be implantable, its size is mostly predetermined, essentially fixing the pressure difference the pump can achieve. Passive valves are used to control the direction of flow inside the micropump. The valve must open when the micropump is active, and close when inactive to prevent any backflow from occurring. In other words, the valve has to be light enough to open with the limited pressure difference, and heavy enough to close properly. These contradictory requirements necessitate careful design of the valve. Using MPM, the fluid-structure interactions are solved and the fluid-solid interface is tracked. The valve dynamics are analyzed for different valve lengths to determine its effect on the efficacy of the micropump. The MPM scheme used for this work, specifically the Modified Update Stress Last (MUSL), is explained in detail in Section II-A. The geometry, dimensions, and materials of the micropump are provided in Section II-C, and the results of the simulations are discussed in Section III.

II. Methodology

Before a MPM simulation of the micropump is performed, the MPM algorithm will be explained here. Following this the constitutive models for updating the stress in the solid valve and the stress tensor of the fluid are provided. Next the geometry and the material properties of the micropump are given.

A. The MPM algorithm

The material point method is a hybrid Lagrangian-Eulerian method, that is it uses both Lagrangian and Eulerian descriptions simultaneously. The MPM accomplishes this by discretizing the domain using Lagrangian material points and a Eulerian computational grid, also known as a background grid. The material points store the desired information such as mass, position, and velocity, while the background grid serves only as a computational space. An explanation of the methodology will follow, with a visual representation given in Fig. 2. The domain is discretized using n_p material points, where the subscript $p = 1, \ldots, n_p$ indicates the material point. The material points contain information such as the mass m_p and position $\boldsymbol{x}_p^t$, where the superscript t indicates the the time step. Additionally, the background grid is created consisting of n_I number of nodes. The algorithm can be described by four general stages, particle-to-grid, grid update, grid-to-particle, and particle update. Firstly, the material points are initialized with mass m_p, position $\boldsymbol{x}_p^0$, velocity $\boldsymbol{v}_p^0$, the gradient deformation tensor $\boldsymbol{F}_p^0$, volume V_p^0, density ρ_p^0, and stress $\boldsymbol{\sigma}_p^0$ in Fig. 2a. Next, in the particle-to-grid stage (Fig. 2b) the information is mapped from the particles, e.g. $\boldsymbol{v}_p^t$, to the computational grid. Subsequently, in Fig 2c the values obtained from all the material points are used to update the momentum and find new the grid velocities $\boldsymbol{v}_I^{t+\Delta t}$, where the subscript $I = 1, \ldots, n_I$ indicates a grid node. Following, the updated velocity is then mapped back to the material points in the grid-to-particle phase in Fig 2d. Finally, the contributions of the surrounding grid nodes are combined and the point variables are updated in Fig 2e, e.g. $\boldsymbol{v}_p^{t+\Delta t}$. Preparing for the next time step, the particles are moved to their new positions $\boldsymbol{x}_p^{t+\Delta t}$ in Fig. 2f. The grid is reset, that is all nodal values are set to zero, so the process can be started again. A more detailed explanation, including all the equations used in the MPM scheme, is provided in Algorithm 1.

A few notable points in Algorithm 1 will be elaborated upon here, for a more in-depth commentary on each step of the algorithm the reader is referred to [24]. First, notice the material point mass m_p is time independent, because it is never updated throughout the algorithm. This has the benefit of reducing the computational cost, as the mass does not have to be recalculated each step, and the mass conservation condition is automatically satisfied. Next is the use of double mapping, which is used in the Modified Update Stress Last (MUSL) [25] scheme in Algorithm 1. The MUSL scheme first calculates a nodal predictor velocity $\tilde{\boldsymbol{v}}_I^{t+\Delta t}$, which is employed to update the particle velocity $\boldsymbol{v}_p^{t+\Delta t}$. The updated particle velocity is mapped to the grid for the second time to recalculate the nodal velocity $\boldsymbol{v}_I^{t+\Delta t}$, hence the term double mapped. By double mapping during the grid update, a more stable value for the grid velocities and velocity gradients is found [26]. The equation for updating the particle velocity requires some

additional explanation. It consists of two terms, the first term comes from the Particle In Cell (PIC) method and was used in the original MPM [14], and the second term comes from the Fluid Implicit Particle (FLIP) method. The PIC approach is more stable but has a high energy dissipation. The FLIP method has much better energy conservation but suffers from severe numerical noise. A combined approach was proposed by Stomakhin et al. [27] as

$$\begin{aligned}\boldsymbol{v}_p^{t+\Delta t} = (1-\alpha)\Sigma_I \phi_I(\boldsymbol{x}_p^t)\tilde{\boldsymbol{v}}_I^{t+\Delta t} \\ + \alpha(\boldsymbol{v}_p^t + \Sigma_I \phi_I(\boldsymbol{x}_p^t)(\tilde{\boldsymbol{v}}_I^{t+\Delta t} - \boldsymbol{v}_I^t)),\end{aligned} \tag{1}$$

where $0 \leq \alpha \leq 1$, though generally it takes a value between $\alpha = 0.95$ and $\alpha = 0.99$ [26], [27]. The last thing pointed out here, are the basis function $\phi_I(\boldsymbol{x}_p^t)$ and the gradient basis function $\nabla\phi_I(\boldsymbol{x}_p^t)$. There are different choices for the basis function for the MPM method, mainly linear, B-spline, or Bernstein functions. In this work the cubic B-spline function is used, because they were found to provide more stable solutions [28], [29]. The fluid-structure interface in MPM is tracked using the computational grid. The fluid and solid material points are mapped to the same grid. A no-slip boundary condition is automatically applied to the interface and the results are subsequently interpolated back to the material points. This makes tracking the interface in MPM relatively easy, unlike in meshbased methods where the mesh needs to continually deform to track the interface.

B. Constitutive models

The stresses in Algorithm 1 are determined by a constitutive model. The valve is modeled as an elastic material. The stress tensor for an isotropic linearly elastic material is given by

$$\boldsymbol{\sigma} = \lambda \text{tr}\boldsymbol{\varepsilon}\mathbf{I} + 2\mu\boldsymbol{\varepsilon}, \tag{2}$$

where λ and μ are the Lamé's constants given by the Young's modulus E and the Poisson ratio ν as

$$\lambda = \frac{E\nu}{(1+\nu)(1-2\nu)}, \quad \mu = \frac{E}{2(1+\nu)}. \tag{3}$$

The constitutive model for the fluid determined the stress by [30]

$$\boldsymbol{\sigma}^f = 2\mu^f \dot{\boldsymbol{\varepsilon}} + \lambda^f \text{tr}\dot{\boldsymbol{\varepsilon}} - \hat{p}\mathbf{I}, \tag{4}$$

where μ^f is the viscosity and λ^f the bulk viscosity. The superscript f is used denote the fluid domain, in order to differentiate the fluid and solid variables. The pressure $\hat{p}$ is given as [31]

$$\hat{p} = K\left[\left(\frac{\rho}{\rho_0}\right)^\gamma - 1\right], \tag{5}$$

where K is the bulk modulus, γ the heat capacity ratio and ρ_0 indicates the initial density.

C. The micropump

The micropump for nerve injury treatment is simulated using the MPM algorithm described in Section II-A. The pump consists of a lower and upper chamber separated by a valve. When closed the valve tip rests on the valve seat and prevents any backflow from occurring. The dimensions of the micropump are given in Table I, for which the length of the valve is varied over multiple simulations between $300\,\mu m$ and $360\,\mu m$. The material properties for the fluid, i.e. air, and the solid valve are provided in Table II. The options for a suitable material for the micropump are limited, due to the requirements that the material is biocompatible and can be fabricated using conventional microfabrication processes. The biocompatible requirement, meaning the material is non-toxic and causes no harmful effects to the body, arises from the plans to implant the device in tissue in the future. A suitable material was found in Poly-L-Lactic Acid (PLLA), which meets the biocompatible requirements while allowing for fabrication. For a more in-depth explanation of the fabrication process can be found in [32], [33].

Algorithm 1: Procedure for (MUSL) [26]

Initialization
  Set up the Carthesian grid, set time $t = 0$
  Set up particle data: m_p, $\boldsymbol{x}_p^0$, $\boldsymbol{v}_p^0$, $\boldsymbol{\sigma}_p^0$, $\boldsymbol{F}_p^0$, V_p^0, ρ_p^0
while $t < t_{end}$ **do**
  Point to grid
    Compute nodal mass $m_I^t = \Sigma_p \phi_I(\boldsymbol{x}_p^t) m_p$
    Compute nodal momentum $(m\boldsymbol{v})_I^t = \Sigma_p \phi_I(\boldsymbol{x}_p^t)(m\boldsymbol{v})_p^t$
    Compute nodal force $\boldsymbol{f}_I^t = \Sigma_p[\phi_I(\boldsymbol{x}_p^t) m_p \boldsymbol{b}(\boldsymbol{x}_p^t) - V_p^t \boldsymbol{\sigma}_p^t \nabla\phi_I(\boldsymbol{x}_p^t)]$
  Grid update with double mapping
    Update momenta $(m\tilde{\boldsymbol{v}})_I^{t+\Delta t} = (m\boldsymbol{v})_I^t + \Delta t \boldsymbol{f}_I^t$
    Apply boundary conditions e.g $(m\tilde{\boldsymbol{v}})_{I_b}^{t+\Delta t} = \mathbf{0}$
    Calculate nodal velocity $\tilde{\boldsymbol{v}}_I^{t+\Delta t} = (m\tilde{\boldsymbol{v}})^{t+\Delta t}/m_I^t$
    Update Particle velocity $\boldsymbol{v}_p^{t+\Delta t} = (1-\alpha)\sum_I \phi_I(\boldsymbol{x}_p^t)\tilde{\boldsymbol{v}}_I^{t+\Delta t} + \alpha(\boldsymbol{v}_p^t \sum_I \phi_I(\boldsymbol{x}_p^t)(\tilde{\boldsymbol{v}}_I^{t+\Delta t} - \boldsymbol{v}_I^t))$
    Update grid momentum $(m\boldsymbol{v})_I^{t+\Delta t} = \Sigma_p \phi_I(\boldsymbol{x}_p^t)(m\boldsymbol{v})_p^{t+\Delta t}$
    Reapply boundary conditions, e.g. $(m\boldsymbol{v})_{I_b}^{t+\Delta t} = \mathbf{0}$
    Nodal velocities $\boldsymbol{v}_I^{t+\Delta t} = (m\boldsymbol{v})^{t+\Delta t}/m_I^t$
  Grid to Particle
    Gradient velocity $\boldsymbol{L}_p^{t+\Delta t} = \Sigma_I \nabla\phi_I(\boldsymbol{x}_p^t)\boldsymbol{v}_I^{t+\Delta t}$
    Gradient deformation tensor $\boldsymbol{F}_p^{t+\Delta t} = (\boldsymbol{I} + \boldsymbol{L}_p^{t+\Delta t})\boldsymbol{F}_p^t$
    Update volume $V_p^{t+\Delta t} = \det(\boldsymbol{F}_p^{t+\Delta t})V_p^0$
    Update stresses (Constitutive model) $\boldsymbol{\sigma}_p^{t+\Delta t} = \boldsymbol{\sigma}_p^t + \Delta\boldsymbol{\sigma}_p$
    Update particle positions $\boldsymbol{x}_p^{t+\Delta t} = \boldsymbol{x}_p^t + \Delta t \Sigma_I \phi_I(\boldsymbol{x}_p^t)\boldsymbol{v}_I^{t+\Delta t}$
  Reset Grid $m_I^t = 0$, $(m\boldsymbol{v})_I^t = \mathbf{0}$, $\boldsymbol{f}_I^t = \mathbf{0}$
  Advance time $t = t + \Delta t$
end

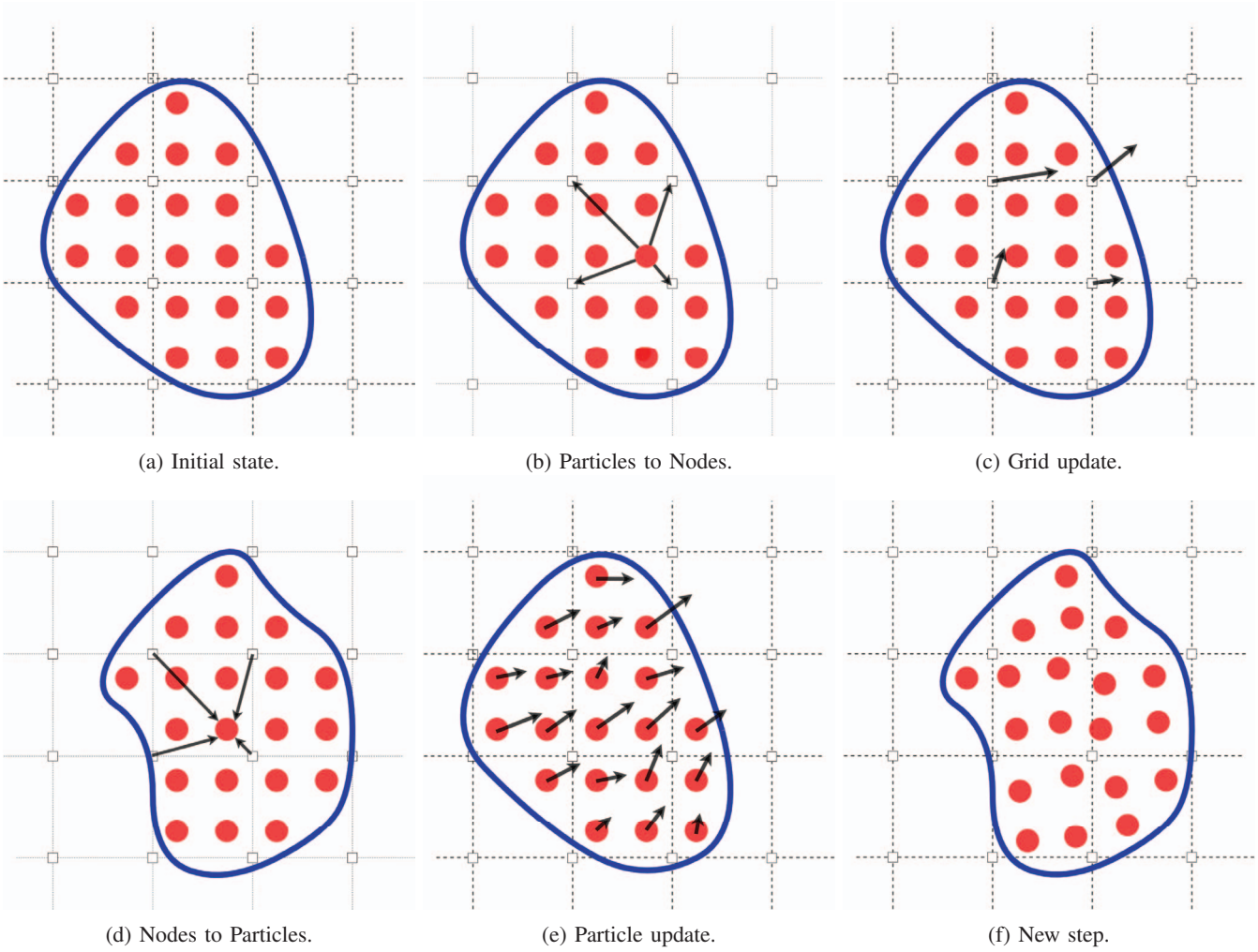

(a) Initial state. (b) Particles to Nodes. (c) Grid update.

(d) Nodes to Particles. (e) Particle update. (f) New step.

Fig. 2: A schematic representation of the material point method.

Section	Dimension $[\mu m]$
Lower chamber height	300
Lower chamber width	300
Upper chamber height	600
Upper chamber width	600
valve thickness	20

TABLE I: Dimensions of the micropump.

Variable	Value
E	12 $[MPa]$
ν	0.4 $[-]$
ρ	1250 $[kg/m^3]$
μ^f	$9.07 \cdot 10^{-5}$ $[Pa\ s]$
γ	1.4 $[-]$
ρ^f	1.293 $[kg/m^3]$
K	90 $[kPa]$

TABLE II: The material properties used in the simulation.

III. Results

The simulation was set up using the dimensions from Table I and the material properties from Table II. The simulations are performed in the open-source MPM software package Karamelo [34]. Multiple simulations are performed for different valve lengths. Key moments of a representative simulation are shown in Fig 5. In Fig 5a the initial state of the micropump is shown. The flow pushes the valve up, but the part of the valve on the valve seat resists moving, as can be seen in Fig 5b. This is because the upward flow velocity near the wall of the valve seat is low, thus there is not much upward velocity to move the valve in that region, causing the valve to stick to the valve seat. As the valve sticks to the valve seat, the pressure below the valve builds up until the force is great enough to overcome the sticking, opening the valve in Fig 5c and allowing the air to flow through the pump. This resistance to open is expected to become greater as the valve length becomes longer, as the section of the valve above the valve seat becomes larger, and the valve itself becomes heavier. To test this, the tip deflection over time has been plotted for a range of valve lengths in Fig 3. The shorter valves are observed to open sooner and show less resistance to opening. The shortest valve of 310 μm exhibits barely any sticking as it is just a bit longer than the channel. The valve tips are seen to move down before

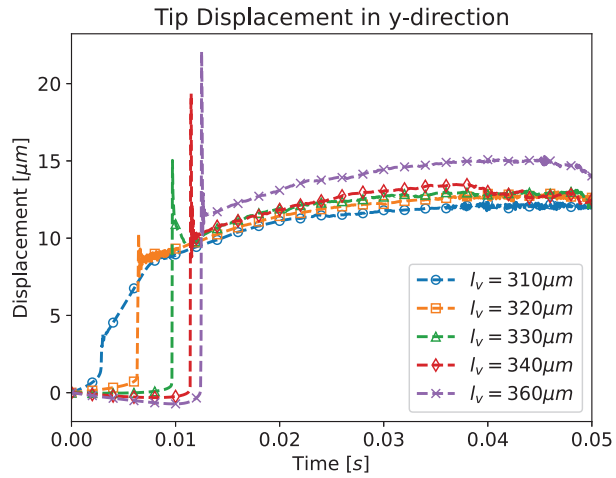

Fig. 3: Tip displacement in y-direction for different valve lengths l_v.

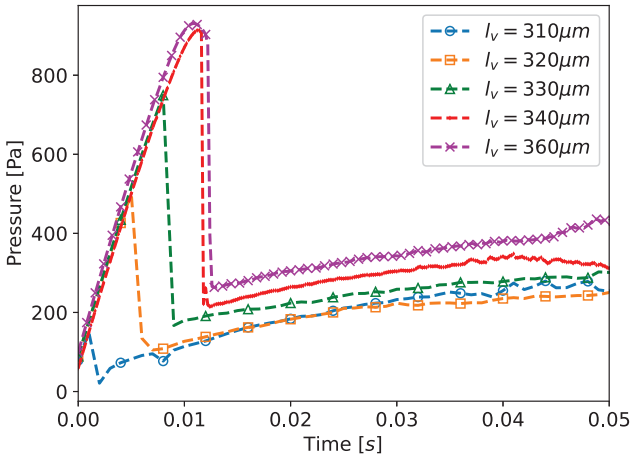

Fig. 4: Pressure below the valve for different valve lengths l_v.

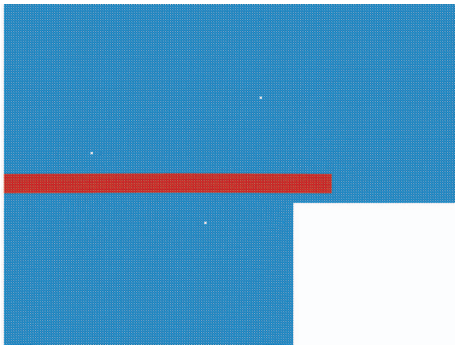

(a) The initial state of the valve.

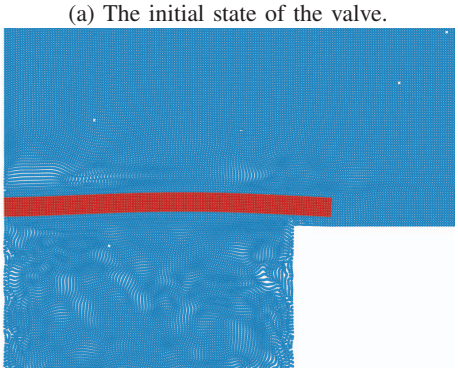

(b) The valve sticking to the valve seat.

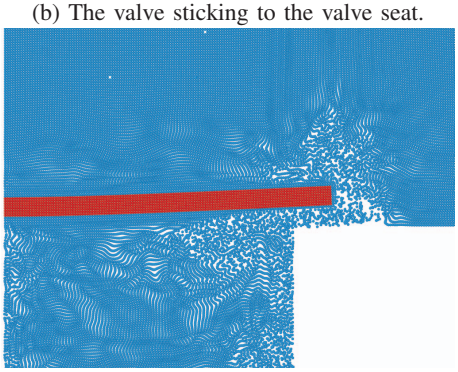

(c) The valve when open.

Fig. 5: The valve at different stages.

going up, this is because the valve bulges as it sticks, as shown in Fig. 5b. Once enough pressure has built up to force the valve open, the valve tip slowly moves up before suddenly shooting up because there is no longer anything holding it close to the valve seat. The air can flow through the open valve, decreasing the pressure and lowering the valve to an equilibrium position in Fig 5c. The pressure below the valve has been plotted for the different valve lengths in Fig. 4. The pressure rises until it drops off and stabilizes when the valve is open for all the different valve lengths. The longer valves are observed to open later compared the the shorter valves. The longer valves also require more pressure to start opening, and to remain open.

IV. Conclusion

In this work, the material point method was employed to simulate a micropump intended for treating peripheral nerve injury. The dynamics of the valve inside the pump are critical to the flow behaviour of the pump. To analyze the effect of the valve length on the behaviour of the valve, fluid-structure interaction have been solved using MPM. By using a set of Lagragian material points and a Eulerian background grid, the meshless MPM can avoid common mesh related issues such as low mesh quality and element deformation. Therefore, it does not need to spend the time meshbased methods such as FEM spend on remeshing, thus improving the total computational cost. Furthermore, the tracking of the fluid-structure interface is accomplished with relative ease. The valve is observed to stick to the valve seat before opening. Tracking the tip displacement of different valve lengths shows the longer the valve is the longer it takes to open. Similarly, looking at the pressure below the valve, the pressure builds up more for longer valves. Indicating the longer valves require a higher pressure difference to open. These results show that the

meshless MPM can be used to influence the valve design of the micropump.

V. Acknowledgment

This research was carried out as part of the project Circular Circuits (project number N21006) funded by the Dutch Research Council (www.nwo.nl)

References

[1] A. T. Liem, A. B. Ari, C. Ti, M. J. Cops, J. G. McDaniel, and K. L. Ekinci, "Nanoflows induced by mems and nems: Limits of two-dimensional models," *Physical Review Fluids*, vol. 6, no. 2, p. 024201, 2021.

[2] F. Alnaimat, I. M. AlHamad, and B. Mathew, "Heat transfer intensification in mems two-fluid parallel flow heat exchangers by embedding pin fins in microchannels," *International Journal of Thermofluids*, vol. 9, p. 100048, 2021.

[3] A. Tajeddin, N. Mustafaoglu, and M. K. Yapici, "On-chip measurement of ph using a microcantilever: A biomimetic design approach," in *2021 Symposium on Design, Test, Integration & Packaging of MEMS and MOEMS (DTIP)*. IEEE, 2021, pp. 01–05.

[4] D. S. Vishnampet, S. Yenuganti, S. Paliwal, M. Peparthi, and K. Panneerselvam, "Design and simulation of a resonance-based mems viscosity sensor," *Journal of Computational Electronics*, vol. 23, no. 1, pp. 122–130, 2024.

[5] X. Gong, Y.-C. Kuo, G. Zhou, W.-J. Wu, and W.-H. Liao, "An aerosol deposition based mems piezoelectric accelerometer for low noise measurement," *Microsystems & Nanoengineering*, vol. 9, no. 1, p. 23, 2023.

[6] J. Briones, W. Espulgar, S. Koyama, H. Takamatsu, E. Tamiya, and M. Saito, "A design and optimization of a high throughput valve based microfluidic device for single cell compartmentalization and analysis," *Scientific reports*, vol. 11, no. 1, p. 12995, 2021.

[7] T. Sciberras, M. Demicoli, I. Grech, B. Mallia, P. Mollicone, and N. Sammut, "Coupled finite element-finite volume multi-physics analysis of mems electrothermal actuators," *Micromachines*, vol. 13, no. 1, p. 8, 2021.

[8] W. T. Sołowski, M. Berzins, W. M. Coombs, J. E. Guilkey, M. Möller, Q. A. Tran, T. Adibaskoro, S. Seyedan, R. Tielen, and K. Soga, "Material point method: Overview and challenges ahead," *Advances in Applied Mechanics*, vol. 54, pp. 113–204, 2021.

[9] H. Chen, S. Zhao, J. Zhao, and X. Zhou, "Dem-enriched contact approach for material point method," *Computer Methods in Applied Mechanics and Engineering*, vol. 404, p. 115814, 2023.

[10] M. Kardani, M. Nazem, D. Sheng, and J. P. Carter, "Large deformation analysis of geomechanics problems by a combined rh-adaptive finite element method," *Computers and Geotechnics*, vol. 49, pp. 90–99, 2013.

[11] A. Azad, A. A. A. Arani, A. Arefmanesh, and R. Shamsoddini, "Analysis of nanofluid flow and heat transfer inside a channel with smoothed particle hydrodynamics," *International Journal of Thermofluids*, vol. 25, p. 100995, 2025.

[12] R. Vaghefi, "A novel meshless radial basis reproducing kernel particle approach for 3d thermo-mechanical analysis of mushy zone phase-change problems," *International Journal of Heat and Mass Transfer*, vol. 234, p. 126128, 2024.

[13] Y. Kong, S. Zhang, J. Zhang, and Y. Zheng, "Inflow and outflow numerical simulation using least-square moving particle semi-implicit method on gpu," *Computational Particle Mechanics*, vol. 11, no. 2, pp. 627–641, 2024.

[14] D. Sulsky, Z. Chen, and H. L. Schreyer, "A particle method for history-dependent materials," *Computer methods in applied mechanics and engineering*, vol. 118, no. 1-2, pp. 179–196, 1994.

[15] F. H. Harlow, "The particle-in-cell computing method for fluid dynamics," *Methods Comput. Phys.*, vol. 3, pp. 319–343, 1964.

[16] Y. Lian, J. Chen, M.-J. Li, and R. Gao, "A multi-physics material point method for thermo-fluid-solid coupling problems in metal additive manufacturing processes," *Computer Methods in Applied Mechanics and Engineering*, vol. 416, p. 116297, 2023.

[17] R. M. Telikicherla and G. Moutsanidis, "A displacement-based material point method for weakly compressible free-surface flows," *Computational Mechanics*, vol. 75, no. 1, pp. 389–405, 2025.

[18] W.-C. Yang, P. Arduino, G. R. Miller, and P. Mackenzie-Helnwein, "Smoothing algorithm for stabilization of the material point method for fluid–solid interaction problems," *Computer Methods in Applied Mechanics and Engineering*, vol. 342, pp. 177–199, 2018.

[19] N. Spiezia, F. Ceccato, V. Salomoni, and P. Simonini, "Simulation of consolidation in large strains: a comparison between finite element method and material point method," in *COUPLED VI: proceedings of the VI International Conference on Computational Methods for Coupled Problems in Science and Engineering*. CIMNE, 2015, pp. 82–93.

[20] P. Meena, A. Kakkar, M. Kumar, N. Khatri, R. K. Nagar, A. Singh, P. Malhotra, M. Shukla, S. K. Saraswat, S. Srivastava *et al.*, "Advances and clinical challenges for translating nerve conduit technology from bench to bed side for peripheral nerve repair," *Cell and tissue research*, vol. 383, no. 2, pp. 617–644, 2021.

[21] A. Muheremu and Q. Ao, "Past, present, and future of nerve conduits in the treatment of peripheral nerve injury," *BioMed research international*, vol. 2015, no. 1, p. 237507, 2015.

[22] X. Navarro, S. Geuna, C. Grothe, and K. Haastert-Talini, "Introduction: thematic papers issue on peripheral nerve regeneration and repair," *The Anatomical Record*, vol. 301, no. 10, pp. 1614–1617, 2018.

[23] M. S. U. Sahar, T. Mettyas, M. Shah, R. Bindra, and M. Barton, "Histological, immunohistochemical, and morphometric analysis of negative pressure-assisted in-vivo nerve stretch-growth," *Neuroscience Letters*, vol. 782, p. 136687, 2022.

[24] V. P. Nguyen, A. De Vaucorbeil, and S. Bordas, *The Material Point Method Theory, Implementations and Applications*, 2023.

[25] D. Sulsky, S.-J. Zhou, and H. L. Schreyer, "Application of a particle-in-cell method to solid mechanics," *Computer physics communications*, vol. 87, no. 1-2, pp. 236–252, 1995.

[26] A. de Vaucorbeil, V. Phu Nguyen, S. Sinaie, and J. Ying Wu, "Material point method after 25 years: theory, implementation and applications," Tech. Rep., 2019.

[27] A. Stomakhin, C. Schroeder, L. Chai, J. Teran, and A. Selle, "A material point method for snow simulation," *ACM Transactions on Graphics (TOG)*, vol. 32, no. 4, pp. 1–10, 2013.

[28] M. Steffen, R. M. Kirby, and M. Berzins, "Analysis and reduction of quadrature errors in the material point method (mpm)," *International journal for numerical methods in engineering*, vol. 76, no. 6, pp. 922–948, 2008.

[29] B. Chandra, R. Hashimoto, S. Matsumi, K. Kamrin, and K. Soga, "Stabilized mixed material point method for incompressible fluid flow analysis," *Computer Methods in Applied Mechanics and Engineering*, vol. 419, p. 116644, 2024.

[30] Y.-C. Su, J. Tao, S. Jiang, Z. Chen, and J.-M. Lu, "Study on the fully coupled thermodynamic fluid–structure interaction with the material point method," *Computational Particle Mechanics*, vol. 7, pp. 225–240, 2020.

[31] Z. Sun, Z. Huang, and X. Zhou, "Benchmarking the material point method for interaction problems between the free surface flow and elastic structure," *Progress in Computational Fluid Dynamics, an International Journal*, vol. 19, no. 1, pp. 1–11, 2019.

[32] E. Aprea, F. Pirim, L. Abelmann, P. M. Sarro, and C. Boutry, "A biodegradable, magnetically actuated micropump for peripheral nerve," in *NanoBioTech-Montreux Conference*, 2024.

[33] E. Aprea, F. Pirim, F. Stallone, L. Abelmann, P. M. Sarro, and C. Boutry, "Research trends on biodegradable polymers and composites for biomedical actuators: Towards a biodegradable micropump," in *ICRA@ 40-IEEE International Conference on Robotics and Automation: 40th Anniversary of the IEEE Conference on Robotics and Automation*, 2024.

[34] A. de Vaucorbeil, V. P. Nguyen, and C. Nguyen-Thanh, "Karamelo: an open source parallel c++ package for the material point method," *Computational Particle Mechanics*, vol. 8, pp. 767–789, 2021.